Inorganic Chemistry

Article

pubs.acs.org/IC

Synthetic, Structural, NMR, and Computational Study of a Geminally Bis(*peri*-substituted) Tridentate Phosphine and Its Chalcogenides and Transition-Metal Complexes

Matthew J. Ray, Rebecca A. M. Randall, Kasun S. Athukorala Arachchige, Alexandra M. Z. Slawin, Michael Bühl, Tomas Lebl, and Petr Kilian*

School of Chemistry, EaStChem, University of St Andrews, Fife KY16 9ST, United Kingdom

Supporting Information

ABSTRACT: Coupling of two acenaphthene backbones through a phosphorus atom in a geminal fashion gives the first geminally bis(*peri*-substituted) tridentate phosphine **1**. The rigid nature of the aromatic backbone and overall crowding of the molecule result in a rather inflexible ligand, with the three phosphorus atoms forming a relatively compact triangular cluster. Phosphine **1** displays restricted dynamics on an NMR time scale, which leads to the anisochronicity of all three phosphorus nuclei at low temperatures. Strained bis- and tris(sulfides) **2** and **3** and the bis(selenide) **4** have been isolated from the reaction of **1** with sulfur and selenium, respectively. These chalcogeno derivatives display pronounced in-plane and out-of-plane distortions of the aromatic backbones, indicating the limits of their angular distortions. In addition, we report metal complexes with tetrahedral [(**1**)Cu(MeCN)][BF_4] (**5**), square planar [(**1**)PtCl][Cl] (**6**), trigonal bipyramidal [(**1**)$FeCl_2$] (**7**), and octahedral *fac*-[(**1**)Mo$(CO)_3$] (**8**) geometries. In all of these complexes the tris(phosphine) backbone is distorted, however to a significantly smaller extent than that in the mentioned chalcogenides **2**–**4**. Complexes **5** and **8** show fluxionality in ^{31}P and ^{1}H NMR. All new compounds **1**–**8** were fully characterized, and their crystal structures are reported. Conclusions from dynamic NMR observations were augmented by DFT calculations.

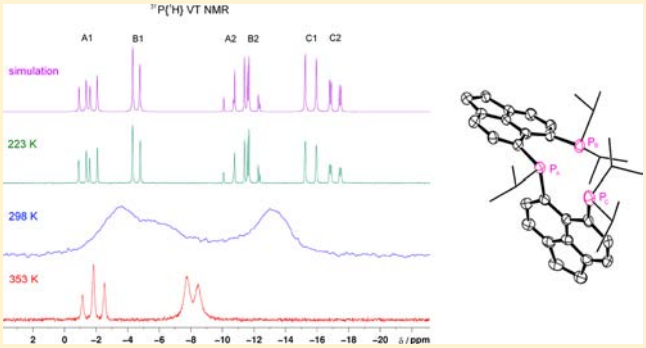

INTRODUCTION

Chelating ligands have been used extensively in coordination chemistry due to the enhanced control of steric and electronic properties, stereochemistry, and coordination number that they give compared to monodentate ligands. The combination of the coordination properties of phosphines and benefits of chelation make tridentate phosphines excellent ligands. Compared with bidentate phosphines, relatively few tridentate phosphines have been reported in the literature, which is surprising considering the advantages bidentate phosphines have over monodentate species in many important homogeneous catalytic processes. Of the tridentate phosphines reported to date, the triphos ligands **A** and **B**[1] are by far the most studied; there are over 300 papers published on various aspects of reactivity of **A** and over 370 on **B**. **B** has provided the basic structure for a number of variations, differing in both the phosphine substituents (**C**, **D**,[2] **E**,[3] **F**[4]) and the bridging chain length (**G**, **H**,[2] **I**[5]) (see Scheme 1). A C-chiral derivative of these ligands (**J**) has also been reported from a modified synthetic method starting from an enantiomerically pure alkyl bromide.[6] A similar strategy was employed in the synthesis of another C-chiral ligand, Pigiphos (**K**),[7] based on a ferrocenylphosphine backbone. Functionalization of both cyclopentadienide rings of ferrocene has been used to synthesize a hexakis(phosphine) ligand that forms binuclear complexes in which it behaves as a tridentate ligand to two metal centers simultaneously (**L**).[8] *Ortho*-substituted phenyl groups are popular structural motifs in tridentate phosphines as their rigidity helps to preorganize the donor atoms into a configuration that favors chelation of a metal. This has been demonstrated in ligands **M**,[9] **N**,[10] **O**,[11] and **P**.[9] A similar motif (based on an indole heterocycle) was utilized in the construction of ligand **Q**.[12] 1,3,5-Tris(phosphino)-substituted cyclohexanes have also been shown to act as tridentate phosphine ligands when in the chair conformation (**R**,[13] **S**,[14] **T**[15]).

Peri-substituted naphthalenes represent another rigid framework potentially useful for the construction of tridentate ligands.[16,17] Schmutzler and others have reported a large series of bis(phosphino)naphthalene ligands, conveniently synthesized by the reaction of 1,8-dilithionaphthalene with 2 molar equiv of a chlorophosphine (Scheme 2).[17−21]

The coordination chemistry of these ligands, and in particular that of 1,8-bis(diphenylphosphino)naphthalene (dppn, R = R′

Received: November 14, 2012
Published: March 27, 2013

   dx.doi.org/10.1021/ic3024875 | *Inorg. Chem.* 2013, 52, 4346−4359

Scheme 1. Selected Tridentate Phosphine Ligands in the Literature[a]

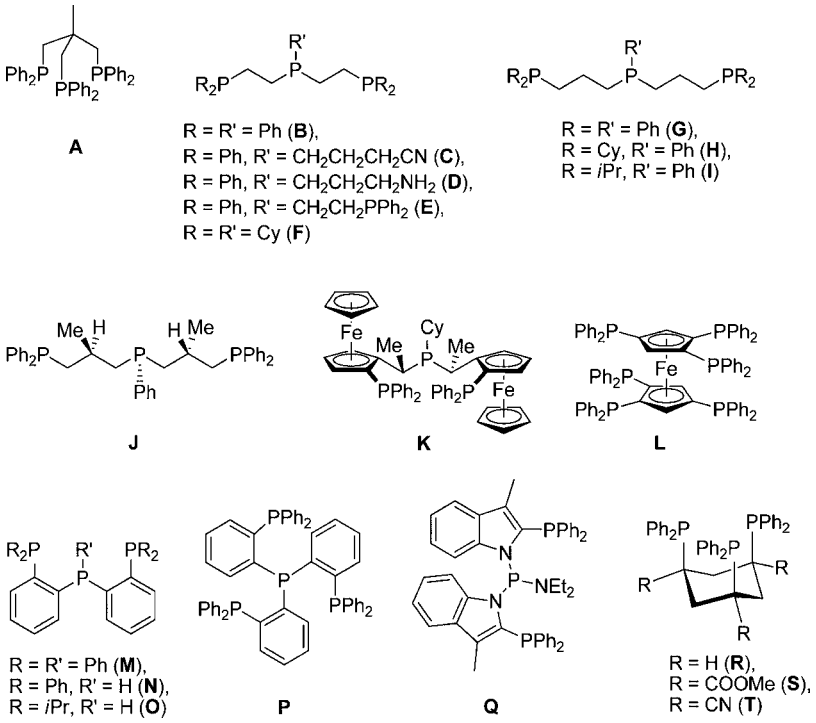

[a]Cy = cyclohexyl.

Scheme 2. Synthesis of 1,8-Bis(phosphino)naphthalenes

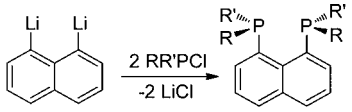

R = R' = Me,[18] Et, *i*Pr, Cy, Ph,[19] NMe_2, NEt_2, $NiPr_2$[20]

R = *t*Bu, R' = Ph[19]

R = Me, R' = C_6F_5[19,21]

= Ph), has been explored extensively. Dppn forms a wide range of complexes with middle and late transition metals with coordination numbers ranging from 3 to 6 and has proven to be an excellent small bite angle ligand due to the unique steric constraints imposed by *peri*-substitution. However, no *tridentate* ligands based on a geminally bis(*peri*-substituted) naphthalene framework have been reported in the literature so far. We report here the synthesis and reactivity of such a tridentate phosphine, **1**, which is the first example of what may potentially develop into a new family of ligands with tight geometrical restraints.

RESULTS AND DISCUSSION

Ligand 1, Sulfides 2 and 3, and Selenide 4. Recently we published the preparation of 5-bromo-6-(diisopropylphosphino)acenaphthene.[22] We now use this compound as the principal starting material in the synthesis of the new tridentate ligand **1** (Scheme 3). First, a lithium–halogen exchange reaction with *n*BuLi in diethyl ether at −78 °C afforded 5-lithio-6-(diisopropylphosphino)acenaphthene. This was without isolation reacted with 1/2 equiv of $iPrPCl_2$ at the same temperature. The salt byproducts were removed by filtration through a sinter with a filtration aid (Celite). After removal of volatiles in vacuo and subsequent washing with acetonitrile, **1** was obtained as a yellow solid in 68% yield in good purity. An optimization of the reaction conditions showed that the yield of **1** was maximized by slow addition of $iPrPCl_2$ and maintaining a low temperature for an extended period after the addition. **1** is air stable as a solid or in solution in organic solvents.

The $^{31}P\{^1H\}$ NMR spectrum of **1** in toluene-d_8 (202.4 MHz, 298 K) shows two broad resonances between +2 and −18 ppm, which implies restricted dynamics of the molecule in solution (Figure 1, spectrum a). The expected AB_2 pattern (δ_A = −1.8 ppm, δ_B = −8.1 ppm; J_{AB} = 140 Hz) was revealed when the sample was heated to 353 K (Figure 1, spectrum b). The observed magnitude of $^4J_{PP}$ coupling in **1** is somehow smaller, however, comparable with that observed by MAS solid-state $^{31}P\{^1H\}$ NMR for dppn (199 Hz).[21] Two ABC patterns in a 58:42 ratio become apparent in the $^{31}P\{^1H\}$ NMR spectrum of **1** at 223 K, suggesting that two rotamers are present in solution (Figure 1, spectrum c). This is supported by the ^{31}P EXSY spectrum, which showed exchange between the two ABC spin systems. The coupling pattern for the two ABC spin systems was simulated (Figure 1, spectrum d). The resulting values are as follows (B denotes the inner phosphorus atom): δ_{B1} = −1.52 ppm, δ_{A1} = −4.53 ppm, δ_{C1} = −15.59 ppm, δ_{B2} = −10.88 ppm, δ_{A2} = −11.87 ppm, δ_{C2} = −17.14 ppm, J_{A1-B1} = 93.9, J_{B1-C1} = 142.3, J_{A1-C1} = 0, J_{A2-B2} = 139.7, J_{B2-C2} = 137.6, J_{A2-C2} = 7.3 Hz).

Detailed line shape analysis, which would yield thermodynamic parameters of hindered rotation processes in a solution of **1**, was not possible due to the complexity of the spin system. However, we were able to observe two coalescence conditions, both for the interchange between the A1B1C1 and A2B2C2 spin systems observed in the slow motion regime. Thus, the C1–C2 pair of resonances coalesce at 259.5 K, which

dx.doi.org/10.1021/ic3024875 | Inorg. Chem. 2013, 52, 4346–4359

Scheme 3. Synthesis of Compounds 1−8

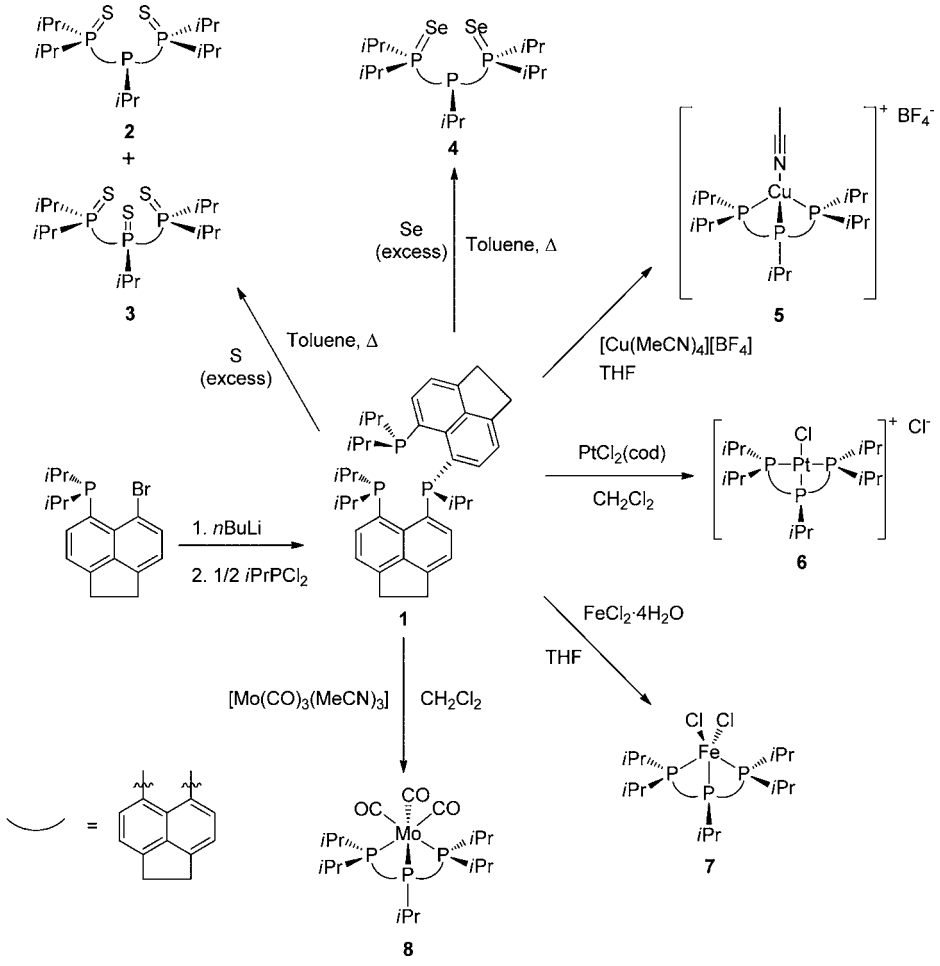

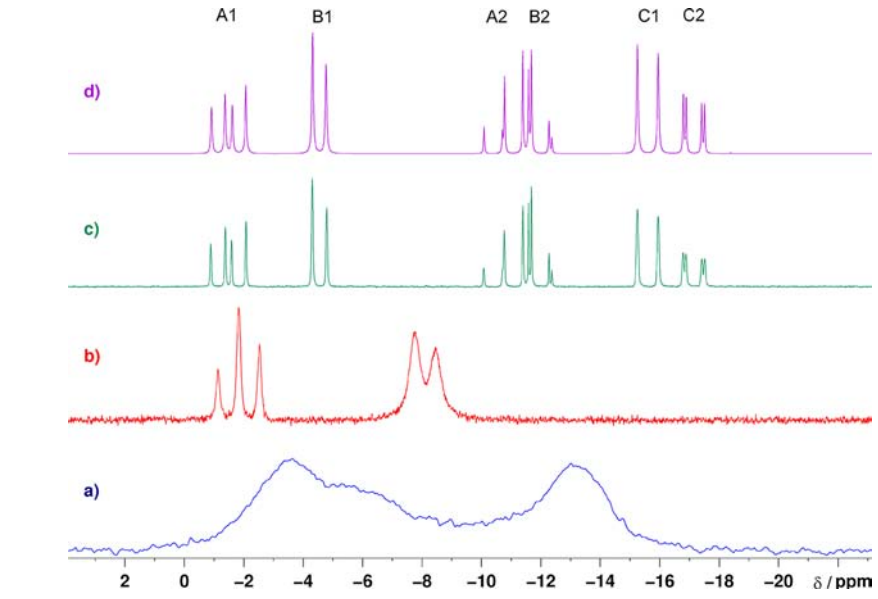

Figure 1. Variable-temperature ^{31}P NMR spectra of **1** in toluene-d_8 at 202.4 MHz: (a) broad resonances at 298 K, (b) AB_2 pattern at 353 K, (c) two ABC patterns in a ratio of 58:42 at 223 K due to two rotamers, (d) simulated ^{31}P coupling pattern with assignments.

corresponds to a barrier of 11.7 kcal mol^{-1}, while the A1−A2 pair of resonances coalesce at 269.4 K with a barrier of 11.4 kcal mol^{-1} (see Table S1 and Figure S1 in the Supporting Information).

Calculations at the B3LYP level indicate that restricted rotation around the P1−C13 bond (see Figure 2 for the numbering of atoms) may correspond to slow interchange between the A1B1C1 and A2B2C2 spin systems observed in

dx.doi.org/10.1021/ic3024875 | Inorg. Chem. 2013, 52, 4346−4359

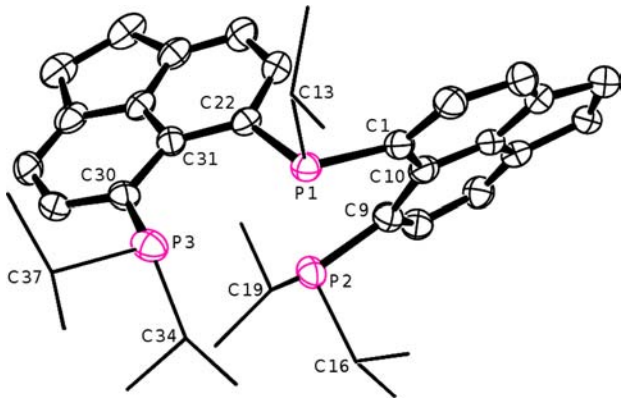

Figure 2. Crystal structure of **1** with ellipsoids drawn at 50% probability. The cocrystallized molecule of MeCN and hydrogen atoms are omitted and *i*Pr groups are shown in stick form for clarity.

^{31}P NMR at low temperature. Two local minima corresponding to the two possible conformers were localized on the potential surface, differing by 0.4 kcal mol^{-1} (B3LYP level, −0.6 kcal mol^{-1} at the B3LYP-D3 level), with a transition barrier of ca. 12 kcal mol^{-1}.[23] The positions of the inner *i*Pr group with respect to the outer phosphorus atoms (P2 and P3) are rather different in the two optimized structures of rotamers, which corresponds well with the observed anisochronicity of P2 and P3 (in ^{31}P NMR) in the two low-temperature ABC spin systems.

In addition to the exchange of the two ABC spin systems observed at low temperature, an additional process takes place which exchanges resonances A and C. This eventually results in an AB$_2$ pattern, which is observed at 353 K (at 202.4 MHz; see Figure 1, spectrum b). We have not succeeded in obtaining the thermodynamic parameters of this process as the faster exchange of the two ABC spin systems "masks" this slower process. We can speculate that the slower exchange process involves rotation around the inner P−C$_{Acenap}$ bonds (P1−C1 and P1−C22).

Interestingly, the related *peri*-substituted bis(phosphines) Nap(P*i*Pr$_2$)$_2$ and Nap(PCy$_2$)$_2$ (Nap = naphthalene-1,8-diyl) exhibit a sharp singlet in their ^{31}P{^{1}H} NMR spectra.[19] This suggests that the rotation around the P−C$_{Nap}$ bonds is relatively unhindered in these compounds, which contrasts sharply with the situation in the geminally bis(*peri*-substituted) ligand **1**.

The crystal structure of **1** (as an acetonitrile monosolvate) is shown in Figure 2, with structural data given in Tables 1 and 4. The molecule of **1** crystallizes in a conformation which brings the three phosphorus atoms into proximity to form a relatively compact triangular P$_3$ cluster. The P···P distances across the *peri*-positions are very similar, 3.17 Å (P1···P2) and 3.15 Å (P1···P3). These are only slightly longer than the respective P···P values observed in Nap(P*i*Pr$_2$)$_2$ (2.944(1) and 2.927(1) Å for the two molecules in the unit cell).[19] The angle between the two acenaphthene mean planes in **1** is 62.0°, which results in the relatively short distance between the two outer phosphorus atoms (P2···P3) of 4.42 Å. Both acenaphthene rings show a similar extent of out-of-plane twist, with the inner P1 atom being 0.23 Å out of the P2-bearing ring mean plane and 0.14 Å out of the P3-bearing ring mean plane. Atoms P2 and P3 are displaced 0.47 and 0.28 Å out of their respective acenaphthene rings. The in-plane distortion of the *peri*-regions in **1** is also comparable to that observed in related 1,8-bis(phosphino)-naphthalenes, the splay angles (Figure 3) in **1** being +15.1° and +12.6° (9.8° and 10.2° in the two molecules in the unit cell of

Table 1. Selected Bond Lengths (Å) and Angles (deg) for 1·MeCN, 2, 3·(CH$_3$)$_2$CO, and 4

	1·MeCN	2	3·(CH$_3$)$_2$CO	4
C1−P1	1.856(6)	1.856(6)	1.830(8)	1.848(5)
C22−P1	1.851(5)	1.856(7)	1.852(8)	1.854(5)
C9−P2	1.836(5)	1.846(6)	1.834(11)	1.850(5)
C30−P3	1.850(5)	1.843(7)	1.849(9)	1.857(5)
P1···P2	3.17	3.61	3.91	3.81
P1···P3	3.15	3.89	4.07	3.69
P2···P3	4.42	6.15	6.19	6.06
P1−S1			1.966(3)	
P2−S/Se2		1.970(3)	1.957(3)	2.1251(12)
P3−S/Se3		1.945(3)	1.972(4)	2.1249(14)
C1−P1−C22	100.94(19)	104.0(3)	106.9(4)	103.67(19)
P1−C1−C10	125.5(4)	122.2(5)	124.0(6)	121.0(3)
C1−C10−C9	128.7(4)	132.2(5)	131.4(8)	131.9(4)
C10−C9−P2	120.9(4)	129.5(5)	126.2(6)	126.6(4)
splay angle (ring bearing P2)[a]	+15.1(4)	+23.9(5)	+21.6(8)	+19.5(4)
P1−C22−C31	123.6(3)	127.2(5)	124.8(6)	122.5(3)
C22−C31−C30	128.5(4)	132.1(6)	131.2(7)	131.5(4)
C31−C30−P3	123.6(4)	131.5(6)	127.4(7)	129.7(3)
splay angle (ring bearing P3)[a]	+12.6(4)	+30.8(6)	+23.4(7)	+23.7(4)

[a]See Figure 3.

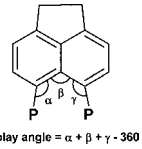

Figure 3. Definition of a splay angle.

Nap(P*i*Pr$_2$)$_2$).[19] The bond angles around the phosphorus atoms in **1** are only slightly more acute vs the ideal tetrahedral angle, with C22−P1−C13 being the most acute at 98.1(3)°.

Reactivity toward chalcogens provides information on the extent of the steric crowding in 1,8-bis(phosphino)-naphthalenes.[24−26] To establish how the extra crowding concomitant with geminal bis(*peri*-substitution) affects the sterics of the phosphorus centers in **1**, we performed a series of reactions with elemental sulfur and selenium.

1 was treated with 3.2 equiv of sulfur in refluxing toluene. This was followed by evaporation of volatiles. The resulting orange oil had a complex ^{31}P{^{1}H} spectrum, indicating that a mixture of products forms. Extraction of the orange oil with hexane and subsequent crystallization from diethyl ether/acetone gave two distinct types of crystals, which were shown to be the bis(sulfide) **2** and tris(sulfide) **3**. The crystals were large enough and formed in sufficiently high quantities to allow for mechanical separation and full characterization by single-crystal X-ray diffraction, ^{1}H, ^{31}P{^{1}H}, and ^{31}P NMR, MS, and elemental analysis. Both **2** and **3** have poor solubility in organic solvents, which prevented acquisition of their ^{13}C{^{1}H} NMR spectra. All signals in the ^{31}P{^{1}H} NMR spectra of **2** and **3** are broadened at 25 °C; the half-width of the peaks is 70−220 Hz for **2** and 15−25 Hz for **3** (both at 121.5 MHz). Thus, **2** displayed three broad singlets at δ_P = 13.3, 73.6, and 84.8 ppm, while **3** exhibited broad singlets at δ_P = 65.7, 68.3, and 84.2 ppm. No fine structure of the peaks (potentially stemming from

dx.doi.org/10.1021/ic3024875 | Inorg. Chem. 2013, 52, 4346−4359

through-space coupling between the ^{31}P nuclei) was observable, presumably due to the broadening. While in the spectrum of **2** it is possible to assign the peak at δ_P = 13.3 ppm to the inner phosphorus atom due to its distinct chemical shift, the similarity in the chemical shifts of P atoms in **3** does not allow similar assignment there with any certainty. The signals in the ^1H NMR spectra of both **2** and **3** were also broadened, which hindered their complete assignment. The $^{31}P\{^1H\}$ NMR spectrum of the crude mixture after reaction showed **2** and **3** were the major components; other phosphorus-containing products were present in smaller amounts. Interestingly, the same distribution of products was observed by $^{31}P\{^1H\}$ NMR when NEt_3 was added to the reaction mixture or when larger excesses of S_8 and/or longer reaction times were used, indicating that the same equilibrium ratio of bis(sulfide) **2** and tris(sulfide) **3** becomes established in all cases. Both **2** and **3** are air stable in the solid state or when dissolved in organic solvents; however, both compounds decompose in chlorinated solvents slowly as indicated by slow darkening of their solutions over several days.

The crystal structures of **2** and **3** (as acetone monosolvates) are shown in Figures 5−7, with structural data given in Tables 1 and 4. The molecule of **2** is significantly more strained than that of **1** due to the increase of steric bulk on thionation of the two outer phosphorus atoms. While the overall geometry of the molecule remains similar to that of **1** (the angle between mean planes of the acenaphthene rings being almost the same, 61.7°), profound changes are seen in all other metric parameters of **2**. The P···P distances are all increased to 3.61 Å (P1···P2), 3.89 Å (P1···P3), and 6.15 Å (P2···P3). The out-of-plane distortions are also increased; P1 is 0.80 and 0.49 Å out of the plane of the two acenaphthene rings, while P3 and P2 are 0.83 and 0.42 Å displaced from their respective acenaphthene mean planes. In the same vein, splay angles (Figure 3) are more obtuse in **2** [+23.9(5)° and +30.8(6)°] than those in **1**.

Differing conformations of the iPr$_2$P(S) groups with respect to the inner P atom (P1) are observed in the structure of **2**. While sulfur atom S3 points approximately toward the *peri*-gap (the C31−C30−P3−S3 dihedral angle is 22.9(6)°), the other sulfur atom S2 points away from its *peri*-gap (the C10−C9−P2−S2 dihedral angle is 154.8(5)°). This results in an approximately linear arrangement of the P1, P2, and S2 atoms, the angle P1···P2═S2 being 174.5°. We also observed slight shortening of the P1···P2 distance vs P1···P3 (3.61 vs 3.89 Å) and slight elongation of the P2−S2 bond distance vs P3−S3 [1.970(3) vs 1.945(3) Å], all this being indicative of a weak donor−acceptor interaction from the lone pair on P1 into the σ^* P2═S2 antibonding orbital (Figure 4). To assess this potential onset of 3c−4e bonding, we computed Wiberg bond indices (WBIs) at the B3LYP/6-31+G* level of density functional theory.[27] However, a barely noticeable WBI of

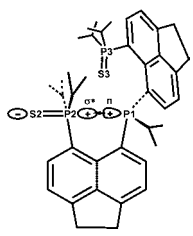

Figure 4. Orbitals involved in weak P1···P2═S2 3c−4e bonding in **2**. Note that the P1···P2═S2 angle is 174.5°.

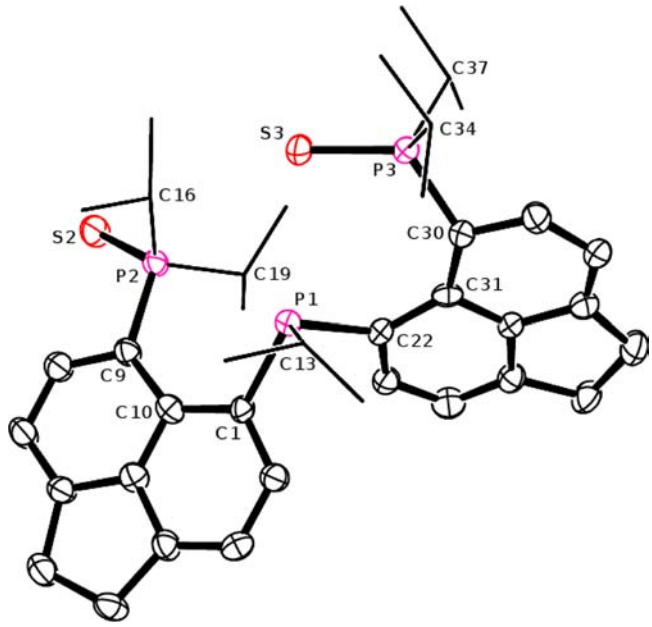

Figure 5. Crystal structure of **2** with ellipsoids drawn at 50% probability. Hydrogen atoms are omitted and *i*Pr groups are shown in stick form for clarity.

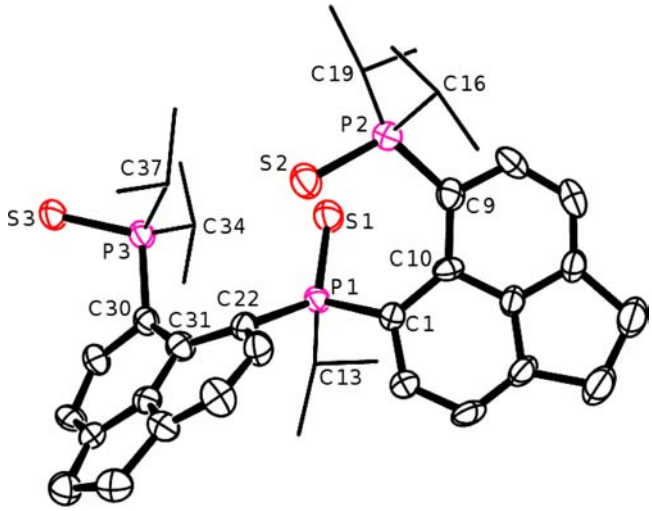

Figure 6. Crystal structure of **3** with ellipsoids drawn at 50% probability. The cocrystallized molecule of acetone and hydrogen atoms are omitted and *i*Pr groups are shown in stick form for clarity.

0.03 is computed between the (inner) P1 and (outer) P2 atoms in **2** (optimized distance 3.70 Å, experimental 3.61 Å).[28] Even more negligible WBIs (below 0.01) were computed between the P1 and P3 atoms in **2** and also between all P atoms in the tris(sulfide) **3**.

As expected, **3** continues the trend of increasing crowding with further thionation. While the angle between the two acenaphthene mean planes is reduced to 52.7°, the P···P distances are elongated to 3.91 Å (P1···P2), 4.07 Å (P1···P3), and 6.19 Å (P2···P3). Notably, the P1···P3 distance is the longest P···P *peri*-distance reported, the previous record being held by the bis(selenide) Nap[P(OiPr$_2$)$_2$Se]$_2$ with a P···P distance of 3.92 Å.[29] The out-of-plane distortions (see Figure 7) are also more pronounced, with the (inner) P1 atom being displaced 1.04 and 1.14 Å from the two acenaphthene mean

dx.doi.org/10.1021/ic3024875 | *Inorg. Chem.* 2013, 52, 4346−4359

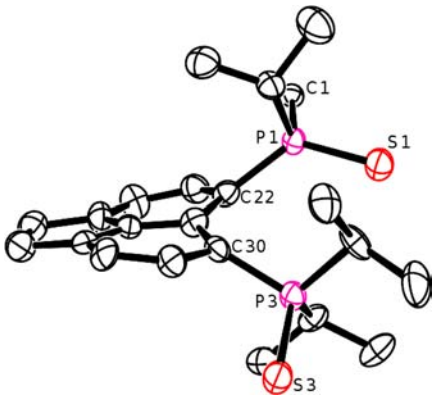

Figure 7. Selected part of a molecule of **3** (in the crystal) illustrating the extent of out-of-plane distortions in the *peri*-region and at the acenaphthene ring. The dihedral angle P1−C22···C30−P3 is 60.1°. Ellipsoids are drawn at 50% probability.

planes, while the P2 and P3 atoms are displaced 1.15 and 1.20 Å from their respective acenaphthene mean planes. The twisting of the actual acenaphthene rings is also very distinct, with atoms C22 and C30 being placed 0.22 and 0.20 Å above and below the mean acenaphthene plane. Interestingly, splay angles [+21.6(8)° and +23.4(7)°; see Figure 3] show that in-plane distortions in **3** are significant, however slightly smaller than in bis(sulfide) **2**.

The reaction of tris(phosphine) **1** with 3.2 equiv of gray selenium was performed in boiling toluene. The $^{31}P\{^{1}H\}$ NMR of the mixture after the reaction was complex; however, recrystallization of the crude product from hexane afforded analytically pure bis(selenide) **4** as yellow needle-shaped crystals in 21.5% yield. The X-ray crystal structure of **4** is shown in Figure 8, with structural data given in Tables 1 and 4.

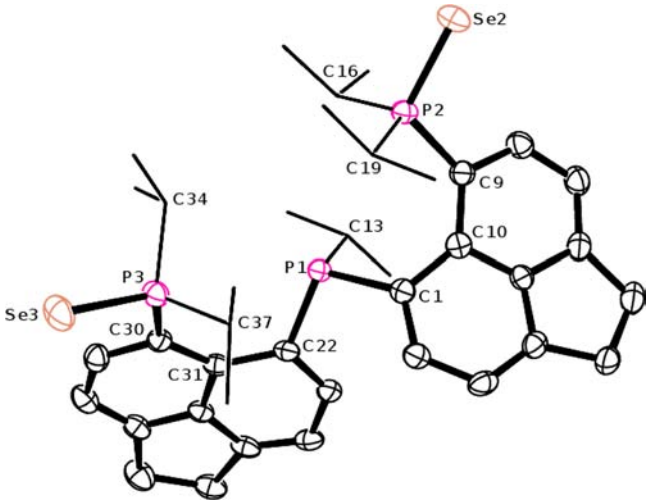

Figure 8. Crystal structure of **4** with ellipsoids drawn at 50% probability. Hydrogen atoms are omitted and *i*Pr groups are shown in stick form for clarity.

The overall geometry of **4** is rather similar to that of bis(sulfide) **2**. The angle between the acenaphthene mean planes is 56.1°, and the *peri*-distances are 3.81 Å (P1···P2), 3.69 Å (P1···P3), and 6.06 Å (P2···P3).

The most contrasting feature of the structure of **4** with regard to **2** is the conformation of the two (outer) $i\mathrm{Pr}_2\mathrm{P(E)}$ (E = S, Se) groups with respect to their respective *peri*-gaps. Thus, both selenium atoms in the structure of **4** are pointing away from the *peri*-gap [C10−C9−P2-Se2, 148.1(3)°; C31−C30−P3−Se3, 151.1(3)°], while in the structure of **2** one of the sulfur atoms points away and one toward the *peri*-gap [C10−C9−P2−S2, 154.8(5)°; C31−C30−P3-S3, 22.9(6)°]. Optimized gas-phase structures of these conformers (B3LYP level) differ in energy only a little; the conformation with both chalcogen atoms in the structure pointing away from the *peri*-gap was found to be more stable in both cases, by 0.9 and 2.4 kcal mol^{-1} for bis(sulfide) **2** and bis(selenide) **4**, respectively. In the X-ray structure of **4** both P1···P2−Se2 and P1···P3−Se3 motifs adopt almost linear arrangements. Such a geometry allows for 3c−4e bonding, with the electron density from the P1 phosphine center being donated to the antibonding σ^* orbital of the P═Se bonds; however, calculations reveal negligible (<0.01) WBIs for these particular interactions.

The $^{31}P\{^{1}H\}$ spectrum of **4** consists of broad singlets (half-width 105−200 Hz at 121.5 MHz) at δ_P = 14.6 ppm (inner P atom) and 78.8 and 86.0 ppm (outer P atoms). Signals in the ^{1}H NMR spectrum were also broadened. As with **2**, poor solubility of **4** in organic solvents prevented characterization by $^{13}C\{^{1}H\}$ and $^{77}Se\{^{1}H\}$ NMR. **4** was further characterized by MS and microanalyses.

Coordination Chemistry of 1. The molecular structure of **1** indicates that the three phosphorus atoms are in an arrangement suitable for cooperative coordination to a single transition-metal center, forming a well-defined coordination pocket. We have indeed isolated complexes of tetrahedral, square planar, trigonal bipyramidal, and octahedral geometries, with **1** acting as a tridentate ligand in each case. These are discussed below.

The reaction of **1** with $[Cu(MeCN)_4][BF_4]$ in thf led to the formation of the complex $[(\mathbf{1})Cu(MeCN)][BF_4]$ (**5**). It was obtained in the form of an air/moisture-sensitive pale yellow powder and was purified by recrystallization from thf. The $^{31}P\{^{1}H\}$ NMR spectrum of **5** exhibits two broad signals at δ_P = −18.7 ppm (br t, inner P) and 6.1 ppm (br s, 2 × outer P). Broadening of the signals (the half-width of both signals is ca. 170−180 Hz at 162.0 MHz) precludes detailed analysis; however, an approximate value of $^{2}J_{PP}$ = 50−60 Hz was read from the spectrum. An interesting feature is that on coordination of **1** to copper(I) (i.e., formation of **5**) the chemical shift of the inner P atom moves toward lower frequency (to δ_P = −18.7 ppm) compared with that in the free ligand (δ_P = −1.4 ppm), which is the opposite direction normally observed on metal coordination. Coordination of triphos (**A**) (δ_P = −27.3 ppm) to copper to form [Cu(triphos)(MeCN)][PF_6] (δ_P = −20.6 ppm)[30] is an example where the opposite trend is observed.

The crystal structure of **5** is shown in Figure 9, with structural data given in Tables 2, 3 and 5. Despite our repeated efforts using a variety of solvents and crystallization techniques, we have only been able to grow relatively small crystals of **5**, which are thin platelets. Hence, our structural data are rather poor; however, they are adequate to demonstrate connectivity and support the assignment of the structure. The molecule crystallizes as a separated cation with a BF_4^- counteranion, together with 1/2 of a solvated molecule of thf. The copper center is tetrahedrally coordinated, with the three phosphine groups of **1** adopting a tripodal geometry and a N-coordinated acetonitrile completing the coordination. The "across *peri*-gap"

dx.doi.org/10.1021/ic3024875 | *Inorg. Chem.* 2013, 52, 4346−4359

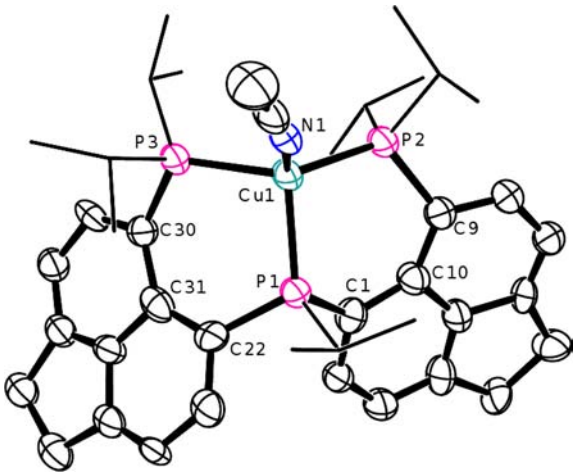

Figure 9. Crystal structure of the cation of **5** with ellipsoids drawn at 50% probability. The BF_4^- counterion, cocrystallized molecule of thf (hemisolvate), and hydrogen atoms are omitted and *i*Pr groups are shown in stick form for clarity.

Table 2. Selected Bond Lengths (Å) and Angles (deg) for $5\cdot{}^1/_2$thf, $6\cdot CH_2Cl_2$, 7·thf, and *fac*-8·MeCN

		$5\cdot{}^1/_2$thf	
P1−Cu1	2.231(3)	P2−Cu1	2.241(3)
P3−Cu1	2.254(3)	N1−Cu1	2.057(8)
P1−Cu1−P2	100.24(9)	P1−Cu1−P3	99.90(9)
P2−Cu1−P3	126.33(10)	P1−Cu1−N1	114.3(3)
P2−Cu1−N1	113.2(2)	P3−Cu1−N1	102.5(3)
		$6\cdot CH_2Cl_2$	
P1−Pt1	2.2146(14)	P3−Pt1	2.3364(15)
P2−Pt1	2.3097(15)	Cl1−Pt1	2.3550(17)
P1−Pt1−P2	95.78(5)	Cl1−Pt1−P1	170.98(5)
P1−Pt1−P3	90.07(5)	Cl1−Pt1−P2	86.21(5)
P2−Pt1−P3	173.43(5)	Cl1−Pt1−P3	88.48(6)
		7·thf	
P1−Fe1	2.4240(12)	Fe1−Cl1	2.2737(14)
P2−Fe1	2.6539(13)	Fe1−Cl2	2.3130(17)
P3−Fe1	2.5453(13)		
P1−Fe1−P2	82.79(4)	P1−Fe1−P3	86.64(4)
P1−Fe1−Cl1	108.05(5)	P1−Fe1−Cl2	130.82(5)
Cl1−Fe1−Cl2	121.02(5)	P2−Fe1−P3	163.44(4)
P2−Fe1−Cl1	95.36(5)	P3−Fe1−Cl1	100.03(5)
P2−Fe1−Cl2	89.31(5)	P3−Fe1−Cl2	87.99(5)
		fac-8·MeCN	
P1−Mo1	2.4855(15)	P2−Mo1	2.5289(17)
P3−Mo1	2.5633(16)	C40−Mo1	1.960(6)
C41−Mo1	1.956(5)	C42−Mo1	1.972(6)
P1−Mo1−P2	82.50(5)	P1−Mo1−P3	82.16(5)
P2−Mo1−P3	104.49(5)	P1−Mo1−C40	176.50(14)
P1−Mo1−C41	100.23(15)	P1−Mo1−C42	91.08(15)
P2−Mo1−C40	96.57(15)	P2−Mo1−C41	91.84(16)
P2−Mo1−C42	169.50(13)	P3−Mo1−C40	94.83(15)
P3−Mo1−C41	163.66(16)	P3−Mo1−C42	82.73(14)
C40−Mo1−C41	83.2(2)	C40−Mo1−C42	90.3(2)
C41−Mo1−C42	81.1(2)		

angles on copper are the most acute [P1−Cu1−P3, 99.90(9)°; P1−Cu1−P2, 100.24(9)°], while the angle P2−Cu1−P3 is the most obtuse at 126.33(10)°. The P−Cu bond lengths in **5** [2.231(3)−2.254(3) Å] are similar to those in the related complex [Cu(triphos)(MeCN)][PF_6] [2.2540(18)−2.2742(17) Å],[30] while the slight elongation of the Cu−N bond in **5** (2.057(8) Å) vs that in the mentioned triphos complex (1.939(5) Å) indicates bonding of MeCN may be slightly more labile in **5**. Coordination of **1** to copper(I) results in overall leveling of the P···P distances within the ligand. Thus, the *peri*-P···P distances (P1···P3 and P1···P2) are both slightly elongated at 3.43 Å, while the P2···P3 separation decreases to 4.01 Å.

Table 3. Selected Nonbonded Distances (Å), Angles (deg), and Displacements (Å) Associated with the Tris(phosphine) Ligands within Complexes $5\cdot{}^1/_2$thf, $6\cdot CH_2Cl_2$, 7·thf, and *fac*-8·MeCN[a]

	$5\cdot{}^1/_2$thf	$6\cdot CH_2Cl_2$	7·thf	*fac*-8·MeCN	1·MeCN
P1···P2	3.43	3.36	3.36	3.31	3.17
P1···P3	3.43	3.22	3.41	3.32	3.15
P2···P3	4.01	4.64	5.15	4.03	4.42
interplanar angle[b]	66.9	46.9	46.8	87.2	62.0
		Splay Angles[c]			
ring bearing P2	16.0(8)	21.2(4)	11.0(4)	19.6(5)	15.1(4)
ring bearing P3	18.3(8)	6.3(5)	22.1(4)	21.4(5)	12.6(4)
		Out-of-Plane Displacements[d]			
P1 (from plane bearing P2)	0.65	0.36	0.69	0.33	0.23
P2	0.77	0.22	1.05	0.25	0.47
P1 (from plane bearing P3)	0.66	0.64	0.37	0.16	0.14
P3	0.68	1.04	0.29	0.32	0.28

[a]Relevant data for free ligand (**1**·MeCN) are included for ease of comparison. [b]Angle between the two acenaphthene mean planes within the molecule. [c]For definition see Figure 3. [d]Displacements of phosphorus atoms from the acenaphthene mean planes.

The reaction of **1** with $PtCl_2$(cod) (cod =1,5-cyclooctadiene) in CH_2Cl_2 gave another ionic complex, [(**1**)PtCl][Cl] (**6**), which was isolated as a colorless air-stable solid in quantitative yield. The $^{31}P\{^1H\}$ and $^{195}Pt\{^1H\}$ NMR spectra of **6** display a complex splitting pattern, which was simulated as an ABCX (A, B, and C = ^{31}P; X = ^{195}Pt) spin system. The $^{31}P\{^1H\}$ NMR spectrum consists of three sets of multiplets (δ_A = 27.5 ppm, δ_B = −6.3 ppm, and δ_C = 12.7 ppm (Figure 10)), while a complex multiplet is observed in the $^{195}Pt\{^1H\}$ NMR spectrum (δ_X = −4656.2 ppm (Figure 11)). The *trans*-$^2J_{PP}$ coupling (J_{AC} = 326.4 Hz) has a significantly larger magnitude than the *cis*-$^2J_{PP}$ coupling ($J_{AB} = J_{BC}$ = 22.0 Hz), and the magnitude of the $^1J_{PPt}$ coupling from the inner phosphorus atom ($^1J_{BX}$ = 3048 Hz) is significantly higher than those from the outer atoms ($^1J_{AX}$ = 2230 Hz, $^1J_{CX}$ = 2270 Hz). Hence, the complexity of this spectrum is largely down to the unexpected anisochronicity of the outer phosphorus atoms (A and C), resulting in observable *trans*-$^2J_{PP}$ coupling and a complex splitting pattern.

The crystal structure of **6** is shown in Figures 12 and 13, with structural data given in Tables 2, 3, and 5. Compound **6** crystallizes as an ion-separated complex cation with a chloride counterion and a cocrystallized molecule of CH_2Cl_2. The platinum atom adopts a square planar geometry with slight distortion toward tetrahedral. Thus, the angles around the central atom are P1−Pt1−Cl1 = 170.98(5)° and P2−Pt1−P3 = 173.45(5)°; atoms P1 and Cl1 lie 0.12 Å above and atoms P2 and P3 lie 0.12 Å below the mean plane through the P1, P2, P3, and Cl1 atoms. Of the bond angles about the Pt center, P1−Pt1−P2 is the most obtuse (95.78(5)°) and Cl1−Pt1−P2 is the most acute at 86.21(5)°. The P−Pt bond lengths are similar to

dx.doi.org/10.1021/ic3024875 | Inorg. Chem. 2013, 52, 4346−4359

Table 4. Crystallographic Data for 1·MeCN, 2, 3·$(CH_3)_2CO$, and 4

	1·MeCN	2	3·C_3H_6O	4
chemical formula	$C_{41}H_{54}NP_3$	$C_{39}H_{51}P_3S_2$	$C_{42}H_{57}OP_3S_3$	$C_{39}H_{51}P_3Se_2$
fw	653.81	676.87	767.01	
cryst dimens/mm	0.10 × 0.10 × 0.05	0.15 × 0.15 × 0.03	0.12 × 0.12 × 0.03	0.18 × 0.06 × 0.02
cryst syst	monoclinic	triclinic	monoclinic	monoclinic
space group	$P2_1/n$	$P\bar{1}$	$P2_1/c$	$P2_1/n$
a/Å	11.898(4)	11.332(4)	16.969(5)	12.3969(13)
b/Å	16.866(6)	12.573(3)	13.057(3)	21.308(3)
c/Å	18.703(7)	13.868(3)	20.051(6)	13.836(2)
α/deg		67.97(2)		
β/deg	99.789(8)	79.63(3)	111.872(6)	92.761(3)
γ/deg		80.50(2)		
V/ Å^3	3698(2)	1791.4(8)	4123(2)	3650.5(7)
Z	4	2	4	4
$D_{calcd/g\ cm^{-3}}$	1.174	1.255	1.236	1.402
μ/cm^{-1}	1.897	3.096	3.275	21.842
no. of reflns measd (unique)	23183 (6678)	15015 (7132)	30878 (7258)	27661 (6396)
R_{int}	0.0894	0.0895	0.1358	0.0677
R1[a]	0.0753	0.0997	0.1317	0.0451
wR2[b]	0.2538	0.3152	0.3340	0.1469

[a] $I > 2\sigma(I)$. R1 = $\sum||F_o| - |F_c||/\sum|F_o|$. [b] wR2 = $\{\sum[w(F_o^2 - F_c^2)^2]/\sum w(F_o^2)^2\}^{1/2}$. $w = 1/[\sigma^2(F_o^2) + [(ap)^2 + bp]]$, where $p = [(F_o^2) + 2F_c^2]/3$.

Table 5. Crystallographic Data for 5, 6·CH_2Cl_2, 7·thf, and *fac*-8·MeCN

	5·$^1/_2$thf	6·CH_2Cl_2	7·thf	*fac*-8·MeCN
chemical formula	$C_{43}H_{58}BCuF_4NO_{0.5}P_3$	$C_{40}H_{53}Cl_4P_3Pt$	$C_{43}H_{59}Cl_2FeO\ P_3$	$C_{44}H_{54}MoNO_3P_3$
fw	840.21	963.68	811.61	833.78
cryst dimens/mm	0.10 × 0.10 × 0.01	0.10 × 0.10 × 0.10	0.12 × 0.12 × 0.12	0.10 × 0.03 × 0.03
cryst syst	monoclinic	triclinic	triclinic	triclinic
space group	$C2/c$	$P\bar{1}$	$P\bar{1}$	$P\bar{1}$
a/Å	30.00(2)	11.288(2)	10.4430(6)	10.962(4)
b/Å	12.361(6)	12.521(2)	11.4725(7)	11.985(4)
c/Å	22.309(11)	16.974(3)	19.353(2)	15.257(5)
α/deg		65.323(7)	93.871(7)	96.390(6)
β/deg	92.409(7)	72.968(9)	101.123(7)	90.902(5)
γ/deg		75.140(9)	112.837(8)	100.702(5)
V/ Å^3	8264(7)	2059.3(6)	2070.6(3)	1956.1(11)
Z	8	2	2	2
$D_{calcd/g\ cm^{-3}}$	1.350	1.554	1.302	1.415
μ/cm^{-1}	6.959	37.964	6.407	4.990
no. of reflns measd (unique)	39144 (7579)	19947 (7441)	20111 (7516)	19925 (7135)
R_{int}	0.2001	0.0736	0.0452	0.0627
R1[a]	0.1825	0.0432	0.0614	0.0655
wR2[b]	0.4874	0.1099	0.1611	0.1470

[a] $I > 2\sigma(I)$. R1 = $\sum||F_o| - |F_c||/\sum|F_o|$. [b] wR2 = $\{\sum[w(F_o^2 - F_c^2)^2]/\sum w(F_o^2)^2\}^{1/2}$. $w = 1/[\sigma^2(F_o^2) + [(ap)^2 + bp]]$, where $p = [(F_o^2) + 2F_c^2]/3$.

those reported in the triphos **B** analogue [Pt(triphos)Cl]Cl,[31] with the inner phosphorus atom in **6** displaying a shorter bond to Pt than the outer atoms [P1−Pt1, 2.2146(14) Å; P2−Pt1, 2.3097(15) Å; P3−Pt1, 2.3364(15) Å], which is in keeping with their respective $^1J_{PPt}$ coupling constants. Notably, due to the more flexible and less crowded ligand, the triphos **B** complex [Pt(triphos)Cl]Cl does not exhibit a significant difference in P−Pt bond length for the outer phosphorus atoms and the two outer phosphorus atoms are isochronous in ^{31}P NMR.

The geometries of the two acenaphthene rings in **6** are rather different. The acenaphthene ring bearing the P2 atom is almost coplanar with the central PtP_3Cl moiety. The out-of-plane distortions of this ring are very moderate; the displacements from the mean acenaphthene plane are 0.36 Å (P1) and 0.22 Å (P2). On the other hand, a significant in-plane strain is present, with a splay angle (Figure 3) of +21.2(4)°. In contrast, the acenaphthene ring bearing the P3 atom shows extensive out-of-plane distortion, with atoms P1 and P3 being displaced by 0.64 and 1.04 Å from their acenaphthene planes. The splay angle for this ring (+6.3(5)°) shows little in-plane distortion is present. Interestingly, the very different types of distortions result in comparable across *peri*-gap distances of P2···P1 = 3.36 Å and P1···P3 = 3.22 Å. The P2···P3 distance is 4.64 Å, and the angle between the two acenaphthene rings is 46.9°. Hence, differing distortions within *peri*-regions of the two acenaphthene units result in variance of the P2−Pt1 and P3−Pt1 bond lengths. These differences are likely to be preserved in the solution, giving a possible explanation for observed anisochronicity of atoms P2 and P3 in the ^{31}P{^{1}H} and ^{195}Pt{^{1}H} NMR spectra of

dx.doi.org/10.1021/ic3024875 | Inorg. Chem. 2013, 52, 4346−4359

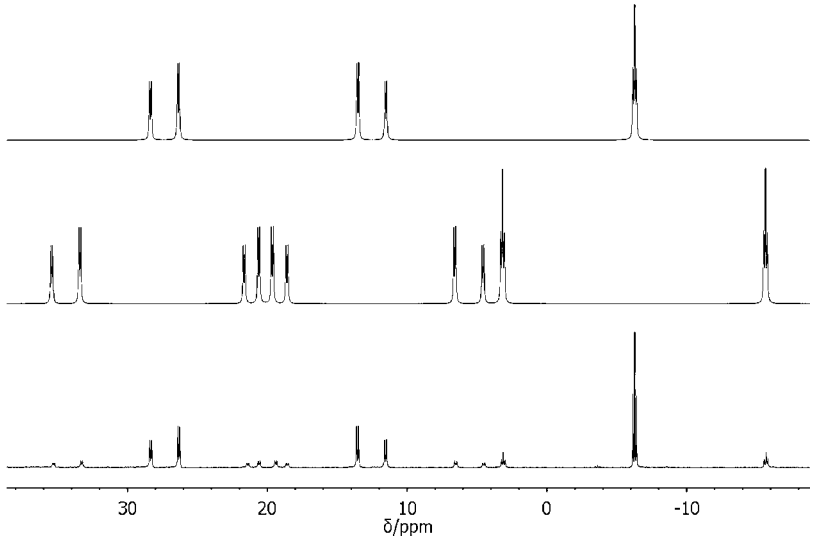

Figure 10. Experimental (bottom) and simulated (top and middle) $^{31}P\{^{1}H\}$ NMR spectra of **6** ($CDCl_3$, 162.0 MHz). The middle spectrum simulates signals of an isotopomer with NMR-active ^{195}Pt nuclei (satellite spectrum), and the top spectrum is from isotopomers with NMR-inactive Pt nuclei.

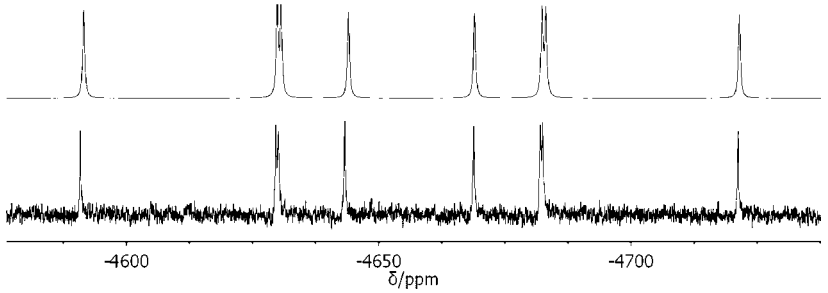

Figure 11. $^{195}Pt\{^{1}H\}$ NMR spectra of **6** (CD_2Cl_2, 58.1 MHz): experimental (bottom) and simulated (top).

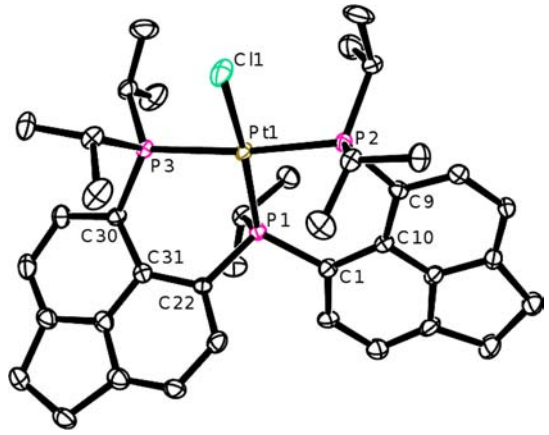

Figure 12. Crystal structure of the cation of **6** with ellipsoids drawn at 50% probability. The chloride counterion, cocrystallized molecule of CH_2Cl_2, and hydrogen atoms are omitted for clarity.

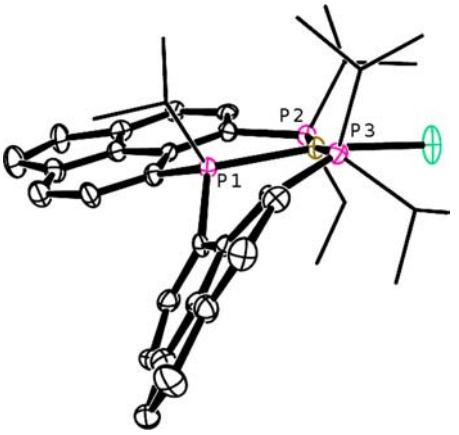

Figure 13. Alternative view of the cation of **6** illustrating differing distortions of the two acenaphthene units. Ellipsoids are drawn at 50% probability. The chloride counterion, cocrystallized molecule of CH_2Cl_2, and hydrogen atoms are omitted and *i*Pr groups are shown in stick form for clarity.

6. The side-on view of the crystal structure of **6** (Figure 13) clearly shows the very different environments of the two outer phosphorus atoms.

Reaction of **1** with $FeCl_2{\cdot}4H_2O$ in thf gave a bright red solution from which [(**1**)$FeCl_2$] (**7**) was isolated as an air-stable red solid. **7** does not show any signals in the NMR spectra,[32] but was fully characterized by X-ray diffraction, IR, and MS, and its purity was established by elemental analysis.

The crystal structure of **7** is shown in Figure 14, with structural data given in Tables 2, 3, and 5; the complex cocrystallizes with a molecule of thf. The central iron(II) atom adopts a distorted trigonal bipyramidal (tbp) geometry, with atom P1 and the two chloride ligands occupying the equatorial part of the molecule. The corresponding (equatorial) angles are

dx.doi.org/10.1021/ic3024875 | *Inorg. Chem.* 2013, 52, 4346−4359

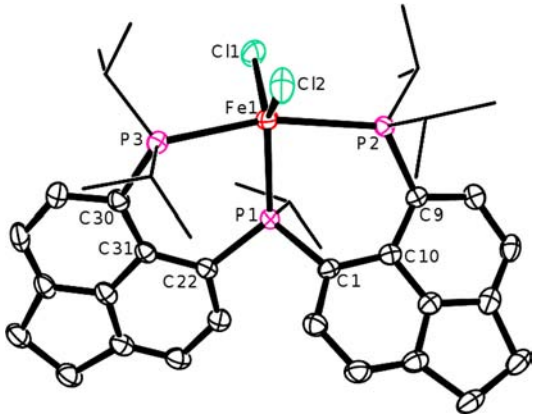

Figure 14. Crystal structure of **7** with ellipsoids drawn at 50% probability. The cocrystallized molecule of thf and hydrogen atoms are omitted and *i*Pr groups are shown in stick form for clarity.

P1−Fe1−Cl1 = 108.05(5)°, P1−Fe1−Cl2 = 130.82(5)°, and Cl1−Fe1−Cl2 = 121.02(5)°. Atoms P2 and P3 adopt axial positions, with the P2−Fe1−P3 angle being 163.44(4)°. All three Fe−P bond lengths differ slightly from each other; the equatorial P1−Fe1 is the shortest at 2.4240(12) Å, and the two axial bonds are elongated to 2.6539(13) (P2−Fe1) and 2.5453(13) Å (P3−Fe1).

The P···P distances across the *peri*-gap [P1···P2, 3.36 Å; P1···P3, 3.41 Å] are (like in **5** and **6**) only slightly elongated with respect to the free ligand **1**; the P2···P3 distance in **7** is 5.15 Å. The overall structural changes adopted by the ligand to form square planar and trigonal bipyramidal complexes **6** and **7**, respectively, are very similar.

Complex **7** represents the first structurally characterized tbp iron complex with three phosphorus and two halide ligands. Structural data of a number of octahedral complexes with four phosphorus and two halide ligands have been reported; these generally contain a pair of bidentate phosphine ligands.

The molybdenum complex [(**1**)Mo(CO)$_3$] (**8**) was obtained from the reaction of **1** with [Mo(CO)$_3$(MeCN)$_3$] in CH_2Cl_2. The major peaks in the $^{31}P\{^1H\}$ NMR spectrum of **8** are a triplet at δ_P = 32.0 ppm and a doublet at δ_P = 35.0 ppm, $^2J_{PP} \approx$ 31 Hz (top spectrum in Figure 15). The $^{31}P\{^1H\}$ NMR spectrum of the same sample at 185 K (bottom spectrum in Figure 15) displayed four broad multiplets at δ_P = 27.6−29.1, 30.9−31.5, 32.5−33.2, and 33.3−34.4 ppm in an approximate integral ratio of 2:1:1:2. The ^{31}P EXSY spectrum at 185 K showed that all four of these multiplets are exchanging, which is consistent with two different isomers of **8** being present in the solution. Given that even at 185 K the spectrum was very broad, we have been unable to deduce further structural or thermodynamic information from it.

Notably, a facile room temperature transformation between *fac*- and *mer*-isomers was observed previously in tricarbonylmolybdenum complexes in solution.[33] Since such an exchange would be consistent with our NMR observations, we have performed a computational investigation in this respect. Our computations indicated that *fac*- and *mer*-isomers of **8** are relatively close in energy. A representative *mer*-isomer was located (B3LYP/6-31+G* level) and turned out to be ca. 4 kcal mol^{-1} less stable that the *fac*-isomer (see Table S3 in the Supporting Information). Indeed, the more stable *fac*-isomer of **8** was found in the solid state by X-ray diffraction; see below. It should be noted though that the *mer*-arrangement was found in all known related Mo complexes with chelating tris(phosphines).[34]

We have also investigated the energetics of the displacement of one of the outer phosphine donor atoms of the chelating ligand with a molecule of acetonitrile. This was believed to be plausible due to the strain in the coordinated tridentate ligand observed in the solid-state structure of **8** (see below) and the fact that acetonitrile (from cocrystallization) may have been available. However, this process was found to be endothermic by at least 15 kcal mol^{-1} and further disfavored by entropy (see Table S3 in the Supporting Information) and can therefore be safely excluded.

Crystallization from MeCN yielded complex *fac*-**8** as brown crystals (17.5% yield). The crystalline material was used for further characterization by IR and Raman spectroscopy, and the purity was verified by microanalysis. Some of the crystals were of sufficient quality for X-ray diffraction work. The structure of *fac*-**8** is shown in Figure 16, with structural data given in Tables 2, 3, and 5. The complex cocrystallizes with a molecule of MeCN. The geometry around the Mo atom is distorted octahedral, with facial coordination of the tris(phosphine)

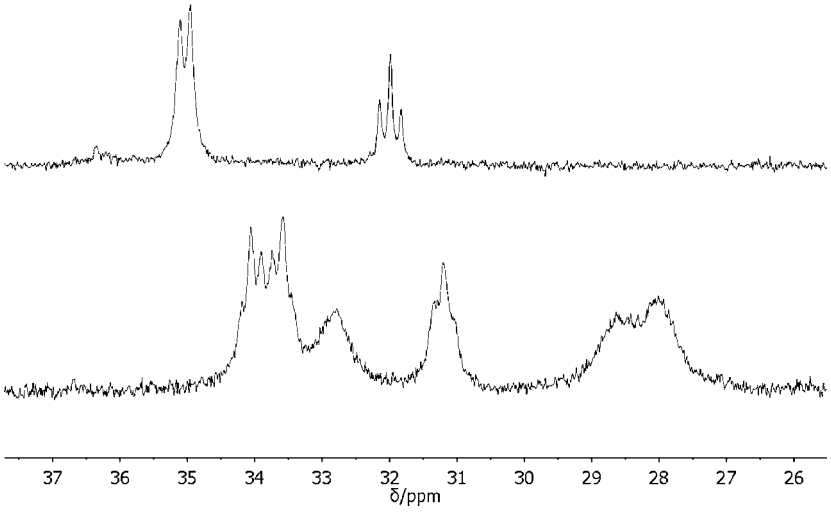

Figure 15. $^{31}P\{^1H\}$ NMR spectra of **8** (CD_2Cl_2, 202.4 MHz) at 298 K (top) and 185 K (bottom).

dx.doi.org/10.1021/ic3024875 | *Inorg. Chem.* 2013, 52, 4346−4359

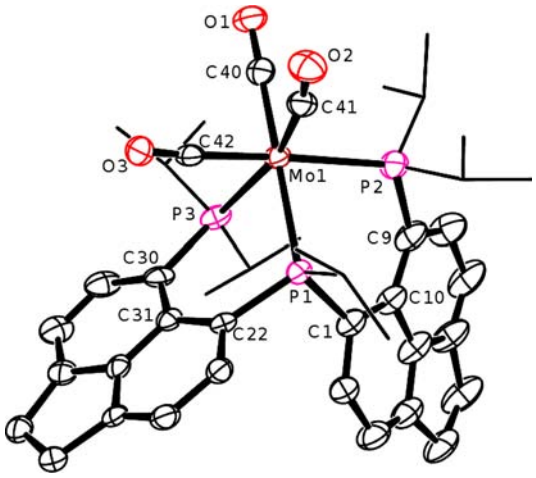

Figure 16. Crystal structure of *fac*-**8**. The cocrystallized molecule of MeCN and hydrogen atoms are omitted and *i*Pr groups are shown in stick form for clarity.

ligand. The tris(phosphine) ligand distortions in *fac*-**8** are essentially limited to those in-plane, resulting in large positive splay angles of +19.6(5)° and +21.4(5)°. The *peri*-distances are slightly increased in *fac*-**8** [P1···P2, 3.31; P1···P3, 3.32 Å] compared with the free ligand **1**, while the P2···P3 separation in *fac*-**8** decreases significantly to 4.03 Å.

CONCLUSION

Despite the rigid nature of the geminal bis(acenaphthene) backbone, the tris(phosphine) ligand **1** accommodates a surprisingly wide range of bonding geometries in both chalcogenides and transition-metal complexes. This is possible via large angular distortions of the *peri*-regions and the independent nature of in-plane and out-of-plane distortions.

Overall, formation of chalcogenides **2**−**4** results in much more "open" structures than formation of the transition-metal complexes **5**−**8**. Thus, while the P···P across *peri*-gap spacings in the chalcogenides range from 3.61 to 4.07 Å, in the transition-metal complexes a range of 3.31−3.43 Å is observed. On the same note, the P2···P3 distances range from 6.06 to 6.19 Å in the chalcogenides **2**−**4**, while they are between 4.01 and 5.15 Å in the series **5**−**8**.

The structure of iron complex **7** and even more so the structure of platinum complex **6** are remarkable in the differing nature of distortions within their two acenaphthene units, one of them showing significant in-plane distortions and much diminished out-of-plane distortions and the other one showing the opposite alterations. The rigidity of the ligand results in all three M−P bonds in each complex **5**−**8** being at least slightly unequal in the crystal, this is in contrast to complexes of the much more flexible triphos family of ligands.

EXPERIMENTAL SECTION

General Procedures. Experiments were carried out under an atmosphere of dry nitrogen using standard Schlenk techniques or under an argon atmosphere using a dry glovebox unless indicated otherwise. Solvents were dried on an MBraun solvent purification system and stored over molecular sieves prior to use. 5,6-Dibromoacenaphthene,[35] 5-bromo-6-(diisopropylphosphino)-acenaphthene,[22] $PtCl_2(cod)$,[36] and $[Mo(CO)_3(MeCN)_3]$[37] were prepared according to literature procedures. *i*PrPCl$_2$ was purchased from Sigma-Aldrich and used without further purification. Where possible, new compounds were fully characterized by ^{31}P, ^{31}P{^{1}H}, ^{1}H, and ^{13}C{^{1}H} NMR, including measurement of ^{1}H{^{31}P}, H−H DQF COSY, H−P HMQC, H−C HSQC, and H−C HMBC experiments. NMR measurements were performed at 25 °C unless otherwise indicated; 85% H_3PO_4 was used as an external standard in ^{31}P, TMS as an internal standard in ^{1}H and ^{13}C NMR. The NMR numbering scheme for compounds **1**−**8** is shown in Scheme 4. NMR spectra

Scheme 4. NMR Numbering Scheme for 1−8

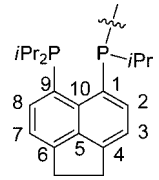

(spin systems) were simulated using the DAISY module in TopSpin 3.1[38] or using MestreNova.[39] Correct isotopic patterns were found in the MS spectra for all assigned peaks.

Tridentate Phosphine 1. *n*BuLi (2.3 mL of 2.5 M solution in hexanes, 5.73 mmol) was added dropwise to the solution of 5-bromo-6-(diisopropylphosphino)acenaphthene (2.0 g, 5.73 mmol) in diethyl ether (80 mL) at −78 °C. The mixture was stirred at −78 °C for 2 h, and then *i*PrPCl$_2$ (0.42 g, 0.37 mL, 2.87 mmol) in diethyl ether (20 mL) was added dropwise over 1 h at −78 °C. The resulting yellow suspension was stirred at −78 °C for 2 h before being warmed to room temperature and stirred for 16 h. The suspension was filtered through a sinter (porosity 3) using a filtration aid (Celite). The solids on the sinter were washed with diethyl ether (40 mL). The volatiles were removed from the filtrate in vacuo to give an orange oil which was stirred with MeCN (20 mL) for 10 min to give a yellow solid suspended in a dark orange solution, the solution containing mainly unreacted starting material. The solid was isolated by filtration and dried in vacuo to give **1** as a yellow powder (1.2 g, 68.0% yield); this material was of sufficient purity for further syntheses. Analytically pure material was obtained by recrystallization from diethyl ether. Large yellow oblong crystals suitable for X-ray diffraction work were grown from MeCN at 2 °C. Anal. Calcd for $C_{39}H_{51}P_3$: C, 76.45; H, 8.39. Found: C, 76.33; H, 8.27. ^{1}H NMR (400.1 MHz, $CDCl_3$): δ = 0.57−1.58 (complex br m, 10 × *i*Pr CH_3, 30H), 1.79−2.32 (br m, 5 × *i*Pr CH, 5H), 3.23−3.37 (m, 2 × CH_2, 4H), 6.91−7.56 (complex br m, 8 × Ar CH, 8H) ppm. Higher temperature ^{1}H NMR spectra in toluene-d_8 displayed additional complexity. ^{31}P{^{1}H} NMR (202.4 MHz, toluene-d_8, 298 K): two broad resonances between δ = +2 and −18 ppm. ^{31}P{^{1}H} NMR (202.4 MHz, toluene-d_8, 353 K): AB_2 system, δ_A = −1.8 ppm, δ_B = −8.1 ppm; J_{AB} = 140 Hz. ^{31}P{^{1}H} NMR (202.4 MHz, toluene-d_8, 223 K): two ABC patterns in a ratio of 58:42 (B denotes the inner phosphorus atom), δ_{B1} = −1.52 ppm, δ_{A1} = −4.53 ppm, δ_{C1} = −15.59 ppm, δ_{B2} = −10.88 ppm, δ_{A2} = −11.87 ppm, δ_{C2} = −17.14 ppm; J_{A1-B1} = 93.9, J_{B1-C1} = 142.3, J_{A1-C1} = 0, J_{A2-B2} = 139.7, J_{B2-C2} = 137.6, J_{A2-C2} = 7.3 Hz. ^{13}C{^{1}H} NMR (67.9 MHz, C_6D_6): δ = 16.9−24.9 (complex br m, *i*Pr CH_3), 25.0−26.8 (br m, *i*Pr CH), 30.3 (s, CH_2), 30.7 (s, CH_2), 31.3−32.1 (br m, *i*Pr CH), 119.3 (s, C3 or C7), 119.5 (s, C3 or C7), 134.8−136.6 (br s, C2 or C8), 135.2 (s, C2 or C8), 147.2 (s, C4 or C6), 148.8 (s, C4 or C6) ppm. Raman (glass capillary, cm^{-1}): ν 3066 (m, νAr−H), 2945 (br m), 2921 (br, s), 2903 (br, m), 2867 (s, νC−H), 1608 (s), 1565 (s), 1444 (s), 1415 (s), 1315 (br, s), 881 (m), 820 (m), 713 (m), 655 (m), 585 (m), 571 (m), 555 (m). IR (KBr disk, cm^{-1}): ν 2944 (s), 2863 (s, νC−H), 1605 (s), 1458 (s), 1380 (m), 1360 (m), 1318 (m), 1256 (m), 1151 (m), 1097 (m), 1032 (s), 878 (m), 839 (s), 819 (s), 651 (m). MS (CI+): *m*/*z* 613.3 (M + H$^+$), 569.3 (M$^+$ − C_3H_7), 343.19 ($C_{21}H_{29}P_2$), 287.16 ($C_{18}H_{24}OP$), 271.17 ($C_{18}H_{24}P$), 135.1. Mp: 181−185 °C.

Reaction of 1 with S_8 to give Sulfides 2 and 3. Powdered sulfur (33 mg, 0.13 mmol) and **1** (0.20 g, 0.33 mmol) in toluene (20 mL) were heated under reflux for 3 h to give an orange solution. Solvent was removed in vacuo to give an orange oil, which was extracted with hexane (20 mL), and the solvent was removed in vacuo. The resulting oil was redissolved in diethyl ether/acetone, and the solution was left

dx.doi.org/10.1021/ic3024875 | *Inorg. Chem.* 2013, 52, 4346−4359

to crystallize by slow evaporation in air. This gave crystals of two distinct types, large cubelike orange crystals and small yellow flakes. X-ray crystallography showed the orange crystals to be the bis(sulfide) **2** and the yellow crystals to be the tris(sulfide) **3**. Manual separation of these crystals allowed the isolation of **2** (52 mg, 22.6%) and **3** (41 mg, 17.8%) for full characterization.

Data for Bis(sulfide) 2. Anal. Calcd for $C_{39}H_{51}P_3S_2$: C, 69.20; H, 7.59. Found: C, 69.13; H, 7.60. $^{31}P\{^1H\}$ NMR (121.5 MHz, $CDCl_3$): δ = 13.3 (br s, P*i*Pr), 73.6 (br s, P*i*Pr$_2$), 85.0 (br s, P*i*Pr$_2$) ppm. ^{31}P NMR (121.5 MHz, $CDCl_3$): δ = 13.2 (br s, P*i*Pr), 73.6 (br s, P*i*Pr$_2$), 84.8 (br s, P*i*Pr$_2$) ppm. ^1H NMR (300.1 MHz, $CDCl_3$): δ = −0.30 to +1.95 (complex br m, 10 × *i*Pr CH_3, 30H), 2.41−5.05 (complex br m, 4 × CH_2 and 5 × *i*Pr CH, 13H), 6.85−7.90 (complex br m, 8 × Ar CH, 8H) ppm. MS (ES+): *m*/*z* 699.3 (M + Na^+), 375.2.

Data for Tris(sulfide) 3. Anal. Calcd for $C_{39}H_{51}P_3S_3$: C, 66.07; H, 7.25. Found: C, 65.95; H, 7.33. $^{31}P\{^1H\}$ NMR (121.5 MHz, C_6D_6): δ = 65.7 (br s), 68.3 (br s), 84.2 (br s) ppm. ^{31}P NMR (121.5 MHz, C_6D_6): δ = 65.7 (br s), 68.3 (br s), 84.2 (br s) ppm. ^1H NMR (300.1 MHz, $CDCl_3$): δ = −0.32 to +1.97 (complex br m, 10 × *i*Pr CH_3, 30H), 2.34 (br s, *i*Pr CH, 1H), 2.51−2.85 (complex br m, 4 × CH_2 and 1 × *i*Pr CH, 9H), 3.52−3.80 (br s, *i*Pr CH, 1H), 5.04−5.40 (br s, *i*Pr CH, 2H), 6.50−7.76 (complex br m, 8 × Ar CH, 8H) ppm.

Reaction of 1 with Se to give Bis(selenide) 4. Powdered gray selenium (82.2 mg, 1.06 mmol) and **1** (0.20 g, 0.33 mmol) in toluene (20 mL) were heated under reflux for 3 h to give a dark green suspension. Solvent was removed in vacuo to give a green-gray oil, which was extracted with hexane (20 mL). The resulting yellow solution was concentrated and left to stand at room temperature, which led to deposition of large clusters of yellow needle-shaped crystals of **4**. These were isolated by filtration and dried in vacuo (54 mg, 21.5% yield). Anal. Calcd for $C_{39}H_{51}P_3Se_2$: C, 60.78; H, 6.67. Found: C, 60.88; H, 6.76. $^{31}P\{^1H\}$ NMR (121.5 MHz, $CDCl_3$): δ = 14.6 (br s, P*i*Pr), 78.8 (br s, P*i*Pr$_2$), 86.0 (br s, P*i*Pr$_2$) ppm. ^{31}P NMR (121.5 MHz, $CDCl_3$): δ = 14.4 (br s, P*i*Pr), 78.2 (br s, P*i*Pr$_2$), 86.2 (br s, P*i*Pr$_2$) ppm. ^1H NMR (300.1 MHz, $CDCl_3$): δ = −1.05 to +1.46 (complex br m, 10 × *i*Pr CH_3, 30H), 1.48−1.92 (complex br m, 4 5 × *i*Pr CH, 5H), 3.31−3.49 (br m, 2 × CH_2, 8H), 7.19−7.42 (br m, 8 × Ar CH, 8H) ppm. MS (ES+): *m*/*z* 811.1 (M+O+Na), 795.1 (M + Na), 747.3, 729.1 (M − C_3H_7), 576.2, 569.3 (M-2Se−C_3H_7), 423.1, 381.1, 343.2.

[(1)Cu(MeCN)][BF$_4$] 5. A solution of **1** (0.25 g, 0.41 mmol) in thf (10 mL) was added to a solution of $[Cu(MeCN)_4][BF_4]$ (0.13 g, 0.41 mmol) in thf (5 mL) at room temperature, giving a yellow suspension. After the solution was stirred for 16 h, the volatiles were removed in vacuo to give **5** as a pale yellow powder (0.33 g, quantitative yield). Analytically pure material was obtained by recrystallization from thf. Colorless rod-shaped crystals suitable for X-ray crystallography were grown from thf at 2 °C. Anal. Calcd for $C_{41}H_{54}BCuF_4NP_3$: C, 61.24; H, 6.77; N, 1.74. Found: C, 61.13; H, 6.66; N, 1.86. ^1H NMR (400.1 MHz, CD_3CN): δ = 0.56 (dd, 6H, $^3J_{HP}$ = 16.7 Hz, $^3J_{HH}$ = 6.9 Hz, *i*Pr CH_3), 0.83 (dd, 6H, $^3J_{HP}$ = 12.0 Hz, $^3J_{HH}$ = 6.8 Hz, *i*Pr CH_3), 0.94 (dd, 6H, $^3J_{HP}$ = 16.0 Hz, $^3J_{HH}$ = 6.8 Hz, *i*Pr CH_3), 1.10−1.17 (m, 12H, *i*Pr CH_3), 2.21−2.33 (m, 1H, inner *i*Pr CH), 2.35−2.47 (m, 2H, outer *i*Pr CH), 2.56−2.70 (m, 2H, outer *i*Pr CH), 3.29−3.40 (m, 8H, CH_2), 7.33 (d, 2H, $^3J_{HH}$ = 7.3 Hz, H3), 7.43 (d, 2H, $^3J_{HH}$ = 7.2 Hz, H7), 7.52 (t, 2H, $^3J_{HP}$ = $^3J_{HH}$ = 7.5 Hz, H2), 7.81 (t, 2H, $^3J_{HP}$ = $^3J_{HH}$ = 7.1 Hz, H8) ppm. $^{31}P\{^1H\}$ NMR (162.0 MHz, CD_3CN): δ = −18.7 (br t, *i*PrP), 6.1 (br s, 2 × *i*Pr$_2$P) ppm, $^2J_{PP}$ = 50−60 Hz. ^{31}P NMR (162.0 MHz, CD_3CN): δ = −18.7 (br m, *i*PrP), 6.1 (br m, 2 × *i*Pr$_2$P) ppm. $^{13}C\{^1H\}$ NMR (75.5 MHz, CD_3CN): δ = 17.5 (s, *i*Pr CH_3), 18.2 (s, *i*Pr CH_3), 19.8 (m, *i*Pr CH_3), 20.1 (d, $^2J_{CP}$ = 11.5 Hz, *i*Pr CH_3), 20.5 (m, *i*Pr CH_3), 24.8−25.3 (m, outer *i*Pr CH), 30.4 (s, CH_2), 30.6 (s, CH_2), 33.1−33.4 (m, central *i*Pr CH), 120.0 (s, C7), 120.2 (d, $^3J_{CP}$ = 4.1 Hz, C3), 120.4−120.8 (m, C10), 123.6 (d, $^1J_{CP}$ = 14.0 Hz, C9), 136.0 (s, C8), 136.6 (s, C2), 140.0−140.5 (m, C1), 141.4−141.6 (m, C5), 151.6 (s, C4 or C6), 152.4 (s, C4 or C6) ppm. Raman (glass capillary, cm^{-1}): ν 3074 (m), 2930 (s), 2732 (m), 1984 (m), 1857 (br, m), 1732 (br, m), 1609 (m), 1562 (m), 1504 (br, m), 1444 (m), 1414 (m), 1313 (s), 1124 (br, s), 817 (m), 586 (m). MS (ES+): *m*/*z* 675 (cation$^+$ − MeCN). Mp: 158−161 °C.

[(1)PtCl][Cl] 6. A solution of **1** (0.12 g, 0.20 mmol) in CH_2Cl_2 (8 mL) was added to a suspension of $PtCl_2$(cod) (73 mg, 0.20 mmol) in CH_2Cl_2 (2 mL) to give a yellow solution, which was stirred for 16 h at room temperature. Evaporation of volatiles in vacuo yielded **6** as a white powder (0.18 g, quantitative yield). Recrystallization from CH_2Cl_2/hexane yielded analytically pure material as well as colorless needle crystals suitable for X-ray crystallography. Anal. Calcd for $C_{39}H_{51}Cl_2P_3Pt$: C, 53.31; H, 5.85. Found: C, 53.24; H, 5.79. ^1H NMR (400.1 MHz, $CDCl_3$): δ = 0.10−0.28 (m, 6H, *i*Pr CH_3), 0.58−0.81 (m, 6H, *i*Pr CH_3), 0.96−1.06 (m, 3H, *i*Pr CH_3), 1.10−1.19 (m, 3H, *i*Pr CH_3), 1.40−1.54 (m, 9H, *i*Pr CH_3), 1.58−1.67 (m, 3H, *i*Pr CH_3), 2.97−3.10 (br s, 1H, *i*Pr CH), 3.30−3.40 (m, 3H, *i*Pr CH), 3.41−3.58 (br m, 8H, CH_2), 3.88−4.04 (br s, 1H, *i*Pr CH), 7.33−7.43 (m, 2H, Ar CH), 7.44−7.54 (m, 2H, Ar CH), 7.61 (d, 2H, *J* = 7.3 Hz, Ar CH), 7.87−7.95 (m, 1H, Ar CH), 8.11−8.20 (m, 1H, ArCH) ppm. $^{31}P\{^1H\}$ NMR (162.0 MHz, $CDCl_3$): ABC spin system (A, B, and C = ^{31}P), with ^{195}Pt satellites forming an ABCX spin system subspectrum (A, B, and C = ^{31}P; X = ^{195}Pt), δP_A = 27.5 ppm ($^2J_{AB}$ = 22.0 Hz, $^2J_{AC}$ = 326.4 Hz, $^1J_{AX}$ = 2230.0 Hz, outer P), δP_B = −6.3 ppm ($^2J_{BC}$ = 22.0 Hz, $^1J_{BX}$ = 3048.0 Hz, inner P), δP_C = 12.7 ppm ($^1J_{CX}$ = 2270.0 Hz, outer P). $^{195}Pt\{^1H\}$ NMR (58.1 MHz, CD_2Cl_2): δ_{Pt} = −4656.2 ppm (m, X part of an ABCX spin system; A, B, and C = ^{31}P; X = ^{195}Pt; see $^{31}P\{^1H\}$ NMR). $^{13}C\{^1H\}$ NMR (75.5 MHz, $CDCl_3$): δ = 15.6−16.0 (m, P*i*Pr CH_3), 16.9−17.4 (m, P*i*Pr CH_3), 18.3−19.2 (m, P*i*Pr$_2$ CH_3), 19.5−20.6 (m, P*i*Pr$_2$ CH_3), 24.7 (d, $^1J_{CP}$ = 26.7 Hz, *i*Pr CH), 26.9 (d, $^1J_{CP}$ = 30.4 Hz, *i*Pr CH), 28.1 (d, $^1J_{CP}$ = 31.4 Hz, *i*Pr CH), 30.4 (s, CH_2), 30.6 (s, CH_2), 31.0 (s, CH_2), 31.2 (s, CH_2), 34.5−35.3 (m, *i*Pr CH), 118.7−119.2 (m, C3 or C7), 119.9−120.7 (m, C3 or C7), 135.0 (s, C2 or C8), 135.4 (s, C2 or C8), 137.1 (s, C2 or C8), 138.6 (s, C2 or C8), 152.4 (s, C4 or C6), 153.2 (s, C4 or C6), 154.1 (s, C4 or C6), 155.6 (s, C4 or C6) ppm. IR (KBr disk, cm^{-1}): ν 2961 (s), 2926 (s), 2869 (s, νC−H), 1595 (m), 1460 (m), 1261 (s), 1095 (s), 1037 (s), 804 (s). MS (ES+): *m*/*z* 842.6 (cation$^+$). Mp: 158−163 °C.

[(1)FeCl$_2$] 7. A solution of **1** (0.2 g, 0.33 mmol) in thf (8 mL) was added to a suspension of $FeCl_2{\cdot}4H_2O$ (64 mg, 0.33 mmol) in thf (1 mL) at room temperature, giving a dark red solution almost instantaneously. After the solution was stirred for 3.5 h, the volatiles were removed in vacuo to give **7** as a red powder (0.22 g, 92.0% yield). Red oblong crystals suitable for X-ray crystallography work were grown from thf and diethyl ether at room temperature. Anal. Calcd for $C_{39}H_{51}Cl_2FeP_3$: C, 63.34; H, 6.95. Found: C, 63.31; H, 7.03. IR (KBr disk, cm^{-1}): ν 2959 (s), 2927 (s), 2869 (m, νC−H), 1597 (m), 1461 (m), 1260 (s), 1098 (br s), 1028 (br s), 845 (m), 804 (s). MS (MALDI-TOF+): *m*/*z* 751.2, 738.2 (M+), 719.2, 703.2 (M − Cl^-), 667.3 (**1** + 2O + Na^+), 645.3 (**1** + 2O + H^+), 629.3 (**1** + O + H^+), 601.3 (**1** − *i*Pr + 2O), 585.3 (**1** − *i*Pr + O), 375.2, 359.2, 343.2. Mp: 181−185 °C.

[(1)Mo(CO)$_3$] 8. $Mo(CO)_6$ (86 mg, 0.33 mmol) was refluxed in MeCN (20 mL) for 6 h to give a yellow solution of $[Mo(CO)_3(MeCN)_3]$.[37] The volatiles were removed in vacuo, and CH_2Cl_2 (2 mL) was added, followed by a solution of **1** (0.20 g, 0.33 mmol) in CH_2Cl_2 (6 mL). The initially orange suspension turned dark brown and was stirred for 16 h and then filtered. The volatiles were removed from the filtrate in vacuo to give crude **8** as a cream solid. Recrystallization from MeCN gave *fac*-**8** in the form of cube-shaped brown crystals (48 mg, 17.5% yield). Anal. Calcd for $C_{44}H_{54}MoNO_3P_3$ (MeCN solvate): C, 63.38; H, 6.53; N, 1.68. Found: C, 62.75; H, 6.53; N, 1.60. ^1H NMR (499.9 MHz, CD_2Cl_2): δ = 0.51−1.63 (complex br m, 10 × *i*Pr CH_3, 30H), 1.68−1.87 (br m, 2 × *i*Pr CH, 2H), 2.66−2.94 (br m, 2 × *i*Pr CH, 3H), 3.32−3.47 (complex br m, 4 × CH_2, 8H), 7.17−7.87 (complex br m, 8 × Ar CH, 8H) ppm. $^{31}P\{^1H\}$ NMR (202.4 MHz, CD_2Cl_2, 298 K): δ = 32.0 (br t), 35.0 (br d) ppm, $^4J_{PP}$ ≈ 31 Hz. $^{31}P\{^1H\}$ NMR (202.4 MHz, CD_2Cl_2, 185 K): δ = 27.6−29.1 (br m), 30.9−31.5 (br m), 32.5−33.2 (br m), 33.3−34.4 (br m) ppm. Raman (glass capillary, cm^{-1}): ν 3071 (m), 2925 (s, νC−H), 1811 (br, νC−O), 1610 (m), 1563 (m), 1443 (m), 1415 (m), 1314 (s), 584 (m). IR (KBr disk, cm^{-1}): ν 2905 (s, br), 2874 (m, νC−H) 1937 (s, νC−O), 1842 (s, νC−O), 1632 (m), 1453 (br, m), 1316 (m), 1037 (m), 853 (m), 832 (m), 632 (m).

dx.doi.org/10.1021/ic3024875 | *Inorg. Chem.* 2013, 52, 4346−4359

X-ray Experimental Details. Tables 4 and 5 list details of the data collection and refinement. Data for compound **1** were collected at −180(1) °C by using a Rigaku MM007 high-brilliance RA generator and Mercury charge-coupled device (CCD) system using ω and φ scans. Data for **2** and **3** were collected at −148(1) °C on the St Andrews robotic diffractometer, a Rigaku ACTOR-SM with a Saturn 724 CCD area detector using ω steps accumulating area detector images spanning at least a hemisphere of reciprocal space. Data for compounds **4**−**8** were collected at −180(1) °C by using a Rigaku MM007 high-brilliance RA generator with a Saturn 70 CCD area detector using ω scans. All instruments use Mo Kα radiation (λ = 0.71075 Å). Intensities were corrected for Lorentz polarization and for absorption. The structures were solved by direct methods. Refinements were done by full-matrix least-squares based on F^2 using SHELXTL.[40] The structures of **3** and **5** while satisfactory for proof of connectivity are of low quality. In both cases repeated attempts yielded very poor crystals, often highly twinned and with high degrees of solvation. The results presented here were from the best samples measured after several attempts. In both cases thin platelets were used for the final determinations.

CCDC 910652−910659 contain the supplementary crystallographic data for this paper. These data can be obtained free of charge via www.ccdc.cam.ac.uk/data_request/cif, by e-mail to data_request@ccdc.cam.ac.uk, or by contacting The Cambridge Crystallographic Data Centre, 12 Union Rd., Cambridge CB2 1EZ, U.K. Fax: +44 1223 336033.

Computational Details. Geometries were fully optimized at the BP86 or B3LYP level of density functional theory (DFT), employing the 962(d) basis on Se, the Stuttgart−Dresden relativistic pseudopotential on Mo (denoted SDD), and the 6-31G* or 6-31+G* basis elsewhere. Energies are reported at the B3LYP/SDD/962(d)/6-31+G* level. For more details and references, see the Supporting Information.

■ ASSOCIATED CONTENT

Supporting Information

CIF files for **1**−**8**, coalescence $^{31}P\{^1H\}$ NMR spectra and relevant thermodynamic data for ligand **1**, and additional computational results and details, including thermodynamic data, plots, and coordinates of optimized structures of conformers of ligand **1** and isomers of complex **8**. This material is available free of charge via the Internet at http://pubs.acs.org.

■ AUTHOR INFORMATION

Corresponding Author

*E-mail: pk7@st-andrews.ac.uk. Fax: +44 1334 463808. Phone: +44 1334 467304.

Notes

The authors declare no competing financial interest.

■ ACKNOWLEDGMENTS

We thank Mrs. C. E. R. Horsburgh at the University of St Andrews and the National Mass Spectrometry Service Centre at the University of Swansea for measurement of mass spectra. We thank the EPSRC, School of Chemistry, EaStChem, and COST action CM0802 PhoSciNet for financial support.

■ REFERENCES

(1) Hewerston, W.; Watson, H. R. *J. Chem. Soc.* **1962**, 1490−1494.
(2) Uriarte, R.; Mazanec, T. J.; Tau, K. D.; Meek, D. W. *Inorg. Chem.* **1980**, *19*, 79−85.
(3) King, R. B.; Kapoor, P. N. *J. Am. Chem. Soc.* **1969**, *91*, 5191−5192.
(4) Yu, J. S.; Rothwell, I. P. *J. Chem. Soc., Chem. Commun.* **1992**, 632−633.
(5) Goikhman, R.; Aizenberg, M.; Ben-David, Y.; Shimon, L. J. W.; Milstein, D. *Organometallics* **2002**, *21*, 5060−5065.
(6) Jia, G.; Man Lee, H.; Williams, I. D. *Organometallics* **1996**, *15*, 4235−4239.
(7) Barbaro, P.; Togni, A. *Organometallics* **1995**, *14*, 3570−3573.
(8) Smaliy, R. V.; Beauperin, M.; Mielle, A.; Richard, P.; Cattey, H.; Kostyuk, A. N.; Hierso, J. *Eur. J. Inorg. Chem.* **2012**, 1347−1352.
(9) Hartley, J. G.; Venanzi, L. M.; Goodall, D. C. *J. Chem. Soc.* **1963**, 3930−3936.
(10) Whited, T. W.; Rivard, E.; Peters, P. C. *Chem. Commun.* **2006**, 1613−1615.
(11) Mankad, N. P.; Rivard, E.; Harkins, S. B.; Peters, J. C. *J. Am. Chem. Soc.* **2005**, *127*, 16032−16033.
(12) Bauer, R. C.; Gloaguen, Y.; Lutz, M.; Reek, J. N. H.; de Bruin, B.; van der Vlugt, J. I. *Dalton Trans.* **2011**, *40*, 8822−8829.
(13) Mayer, H. A.; Otto, H.; Kuehbauch, H.; Fawzi, R. *J. Organomet. Chem.* **1994**, *472*, 347−354.
(14) Mayer, H. A.; Stoessel, P.; Fawzi, R.; Steimann, M. *J. Organomet. Chem.* **1995**, *492*, C1−C3.
(15) Mayer, H. A.; Stoessel, P.; Fawzi, R.; Steimann, M. *Chem. Ber.* **1995**, *128*, 719−723.
(16) Kilian, P.; Knight, F. R.; Woollins, J. D. *Chem.—Eur. J.* **2011**, *17*, 2302−2328.
(17) Kilian, P.; Knight, F. R.; Woollins, J. D. *Coord. Chem. Rev.* **2011**, 1387−1413.
(18) Costa, T.; Schimdbaur., H. *Chem. Ber.* **1982**, *115*, 1374−1378.
(19) Karacar, A.; Thonnessen, H.; Jones, P. G.; Bartsch, R.; Schmutzler, R. *Heteroat. Chem.* **1997**, *53*, 539−550.
(20) Karacar, A.; Freytag, M.; Thonnessen, H.; Jones, P. G.; Bartsch, R.; Schmutzler, R. *J. Organomet. Chem.* **2002**, *643*, 68−80.
(21) Jackson, R. D.; James, S.; Orpen, A. G.; Pringle, P. G. *J. Organomet. Chem.* **1993**, *458*, C3−C4.
(22) Wawrzyniak, P.; Fuller, A. L.; Slawin, A. M. Z.; Kilian, P. *Inorg. Chem.* **2009**, *48*, 2500−2506.
(23) For details see Table S2 in the Supporting Information.
(24) Karacar, A.; Freytag, M.; Thonnessen, H.; Omelanczuk, J.; Jones, P. G.; Bartsch, R.; Schmutzler, R. *Heteroat. Chem.* **2001**, *2*, 102−113.
(25) Omelanczuk, J.; Karacar, A.; Freytag, M.; Jones, P. G.; Bartsch, R.; Mikolajczyk, M.; Schmutzler, R. *Inorg. Chim. Acta* **2003**, *350*, 583−591. Karacar, A.; Freytag, M.; Thonnessen, H.; Omelanczuk, J.; Jones, P. G.; Bartsch, R.; Schmutzler, R. *Z. Anorg. Allg. Chem.* **2000**, *626*, 2361−2372.
(26) Kilian, P.; Slawin, A. M. Z.; Woollins, J. D. *Dalton Trans.* **2003**, 3876−3885.
(27) WBIs are a measure of the covalent character of a bond. They are used routinely to assess bonding interactions between formally nonbonded atoms. See: Wiberg, K. B. *Tetrahedron* **1968**, *24*, 1083−1096.
(28) According to the second-order perturbation analysis in a natural bond orbital (NBO) analysis (Reed, A. E.; Curtiss, L. A.; Weinhold, F. *Chem. Rev.* **1988**, *88*, 899−926) this donor−acceptor interaction is very weak, amounting to just 1 kcal/mol.
(29) Somisara, D. M. U. K.; Bühl, M.; Lebl, T.; Richardson, N. V.; Slawin, A. M. Z.; Woollins, J. D.; Kilian, P. *Chem.—Eur. J.* **2011**, *17*, 2666−2677.
(30) Cain, M. F.; Hughes, R. P.; Glueck, D. S.; Golen, J. A.; Moore, C. E.; Rheingold, A. L. *Inorg. Chem.* **2010**, *49*, 7650−7662.
(31) Sevillano, P.; Habtemariam, A.; Parsons, S.; Castineiras.; Garcia, M. E.; Sadler, P. J. *J. Chem. Soc., Dalton Trans.* **1999**, 2861−2870.
(32) For a discussion of spin states of tbp complexes see Sacconi, L.; Di Vaira, M. *Inorg. Chem.* **1978**, *17*, 810−815.
(33) Cano, M.; Campo, J. A.; Perez-Garcia, V.; Guttierrez-Puebla, E.; Alvarez-Ibarra, C. *J. Organomet. Chem.* **1990**, *382*, 397−406.
(34) All Mo complexes with $RP(CH_2CH_2CH_2PR_2)_2$ ligands, i.e., those with a P−CCC−P−CCC−P backbone similar to that of **8**, that are deposited in the Cambridge Structure Database adopt the *mer* arrangement (seven hits in CSD, version 5.33, November 2012):

(a) Dahlenburg, L.; Pietsch, B. *Chem. Ber.* **1989**, *122*, 2085−2090.
(b) Dahlenburg, L.; Pietsch, B. *Z. Naturforsch.* **1986**, *41b*, 70−75.
(35) Neudorff, W. D.; Lentz, D.; Anibarro, M.; Schlueter, A. D. *Chem.—Eur. J.* **2003**, *9*, 2745−2757.
(36) Drew, D.; Doyle, J. R. *Inorg. Synth.* **1972**, *13*, 47−55.
(37) Miguel, D.; Perez-Martinez, J. A.; Riera, V.; Garcia-Granda, S. *Organometallics* **1994**, *13*, 1336−1340.
(38) *TopSpin*, version 3.1; Bruker BioSpin: Billerica, MA, 2012.
(39) *MestReNova*, version 8.0; Mestrelab Research S.L.: Santiago de Compostela, Spain, 2012.
(40) Sheldrick, G. M. *Acta Crystallogr., Sect. A* **2008**, *64*, 112−122.